



Trehalose-Induced Remodelling of the Human Microbiota Affects *Clostridioides difficile* Infection Outcome in an *In Vitro* Colonic Model: A Pilot Study

OPEN ACCESS

Edited by:

Yolanda López-Vidal,
Universidad Nacional Autónoma de
México, Mexico

Reviewed by:

Mindy Engevik,
Medical University of South Carolina,
United States
Rene Arredondo-Hernández,
National University of Mexico, Mexico
Palok Aich,
National Institute of Science Education
and Research (NISER), India

*Correspondence:

Mark H. Wilcox
mark.wilcox@nhs.net
Anthony M. Buckley
A.Buckley1@Leeds.ac.uk

Specialty section:

This article was submitted to
Microbiome in Health and Disease,
a section of the journal
Frontiers in Cellular and
Infection Microbiology

Received: 26 February 2021

Accepted: 02 June 2021

Published: 02 July 2021

Citation:

Buckley AM, Moura IB, Arai N,
Spittal W, Clark E, Nishida Y,
Harris HC, Bentley K, Davis G,
Wang D, Mitra S, Higashiyama T and
Wilcox MH (2021) Trehalose-Induced
Remodelling of the Human
Microbiota Affects *Clostridioides*
difficile Infection Outcome in an *In Vitro*
Colonic Model: A Pilot Study.
Front. Cell. Infect. Microbiol. 11:670935.
doi: 10.3389/fcimb.2021.670935

Anthony M. Buckley^{1*}, Ines B. Moura¹, Norie Arai², William Spittal¹, Emma Clark¹, Yoshihiro Nishida², Hannah C. Harris¹, Karen Bentley¹, Georgina Davis¹, Dapeng Wang³, Suparna Mitra¹, Takano Higashiyama² and Mark H. Wilcox^{1*}

¹ Healthcare Associated Infection Research Group, Molecular Gastroenterology, Leeds Institute of Medical Research, University of Leeds, Leeds, United Kingdom, ² R&D Division, Hayashibara Co. Ltd./NAGASE Group, Okayama, Japan, ³ LeedsOmics, University of Leeds, Leeds, United Kingdom

Within the human intestinal tract, dietary, microbial- and host-derived compounds are used as signals by many pathogenic organisms, including *Clostridioides difficile*. Trehalose has been reported to enhance virulence of certain *C. difficile* ribotypes; however, such variants are widespread and not correlated with clinical outcomes for patients suffering from *C. difficile* infection (CDI). Here, we make preliminary observations on how trehalose supplementation affects the microbiota in an *in vitro* model and show that trehalose-induced changes can reduce the outgrowth of *C. difficile*, preventing simulated CDI. Three clinically reflective human gut models simulated the effects of sugar (trehalose or glucose) or saline ingestion on the microbiota. Models were instilled with sugar or saline and further exposed to *C. difficile* spores. The recovery of the microbiota following antibiotic treatment and CDI induction was monitored in each model. The human microbiota remodelled to utilise the bioavailable trehalose. Clindamycin induction caused simulated CDI in models supplemented with either glucose or saline; however, trehalose supplementation did not result in CDI, although limited spore germination did occur. The absence of CDI in trehalose model was associated with enhanced abundances of *Fingoldia*, *Faecalibacterium* and *Oscillospira*, and reduced abundances of *Klebsiella* and *Clostridium* spp., compared with the other models. Functional analysis of the microbiota in the trehalose model revealed differences in the metabolic pathways, such as amino acid metabolism, which could be attributed to prevention of CDI. Our data show that trehalose supplementation remodelled the microbiota, which prevented simulated CDI, potentially due to enhanced recovery of nutritionally competitive microbiota against *C. difficile*.

Keywords: *Clostridium difficile*, trehalose, human microbiota, microbial competition, *in vitro* gut model

INTRODUCTION

Trehalose is a disaccharide sugar consisting of two α -glucose monomers linked via 1,1-glycosidic bond and is present in a wide variety of organisms, such as bacteria, yeast, insects, plants, and animals. The structure of trehalose makes it highly resistant to acid hydrolysis, it is used as a high energy storage molecule for insect flight, and also as a dehydration or cryo-protectant in some microorganisms, plants and animals (Elbein et al., 2003). This sugar is naturally found in foods, such as mushrooms and honey, but following the discovery of a cost-effective method of large-scale production (Maruta et al., 1995) and regulatory approval as a food additive, trehalose is now added to a range of processed food products (cereals, pasta, sweets and ice cream), cosmetics and some medicines (Food Standards Australia New Zealand (FSANZ), 2003; Pinto-bonilla et al., 2015). In the human digestive tract, trehalose is metabolised by host-produced trehalase enzymes located at the intestinal brush border, as well as microbial-produced trehalases. Many intestinal bacteria and yeasts produce trehalase enzymes, including *Bacillus* spp., *Escherichia coli*, *Blautia* spp., *Lactobacillaceae* and the nosocomial pathogen *Clostridioides difficile* (Arguelles, 2000; Bateman et al., 2017; Collins et al., 2018a).

C. difficile is the leading cause of antibiotic-associated diarrhoea (Rupnik et al., 2009), where antibiotic-induced microbiota depletion provides favourable conditions for the germination of *C. difficile* spores, which proliferate and produce toxins that cause disease. These toxins (TcdA and TcdB) are responsible for a range of symptoms from mild, self-limiting diarrhoea to pseudomembranous colitis, colonic perforation and death (Rupnik et al., 2009). Antibiotic treatment can fail to resolve the infection, with up to 30% of cases recurring after primary treatment (Marsh et al., 2012). Depletion of the intestinal microbiota means *C. difficile* is exposed to several compounds normally metabolised by the healthy microbiota; some of these are used as either molecular signals or as a source of energy, such as the primary bile acids cholate and succinate (Sorg and Sonenshein, 2008; Ferreyra et al., 2014). Collins et al. showed that ingested trehalose enhanced *C. difficile* virulence (Collins et al., 2018a). Additionally, *C. difficile* ribotypes (RT) typically associated with CDI outbreaks,

e.g. RT027 or RT017, have a mutated *treR* repressor gene, which overexpresses the trehalose metabolism gene (*treA*), whilst other ribotypes, i.e. RT078, show enhanced trehalose uptake, through the presence of a novel phosphotransferase (PTS) system transporter (Collins et al., 2018b). However, it is reported that such variants are common in *C. difficile* isolates and comparison of the clinical outcome of CDI patients to trehalose metabolic genotype of the isolated strain found no correlation between 30-day mortality and the trehalose metabolic genotype (Eyre et al., 2019). Moreover, Saund et al. found no statistically significant association between the presence of trehalose utilisation variants in infecting *C. difficile* strains and the development of severe infection outcome (Saund et al., 2020).

Using a previously successful *in vitro* model developed to simulate human CDI in the large intestine (Freeman et al., 2003), we measured microbial compositional changes following trehalose and glucose supplementation and the effect of sugar supplementation on *C. difficile* growth kinetics after antibiotic disruption of the microbiota. A schematic timeline of our experimental design is shown in **Figure 1**. Enumeration of *C. difficile* from the *in vitro* gut model when predicting treatment and antibiotic induction outcomes have been shown to be clinically reflective, and in some cases, more accurate than results from animal models. Antibiotics with a high propensity to induce CDI in patients also induce simulated CDI within the gut model (Freeman et al., 2003; Saxton et al., 2009; Crowther et al., 2013; Chilton et al., 2014). Conversely, antibiotics with a lower *in vitro* propensity to induce simulated CDI are now recognised to have low CDI risk (Baines et al., 2005; Saxton et al., 2009). Crucially, the gut model has been used for *in vitro* evaluation of drug efficacy against simulated CDI at various stages of pre-clinical and clinical drug development. For fidaxomicin, data from animal and *in vitro* models correlated well with Phase III clinical trials (Swanson et al., 1991; Crook et al., 2012; Chilton et al., 2014), whereas for the toxin binding agent, tolevamer, results from the triple-stage gut model predicted clinical failure of this agent at Phase III, while animal model data did not (Kurtz et al., 2001; Baines et al., 2009; Johnson et al., 2014). Following gut model investigations of cadazolid (Chilton et al., 2014), surotomycin (Chilton et al., 2014) and SMT19969 (Baines et al., 2015) for treatment of CDI,

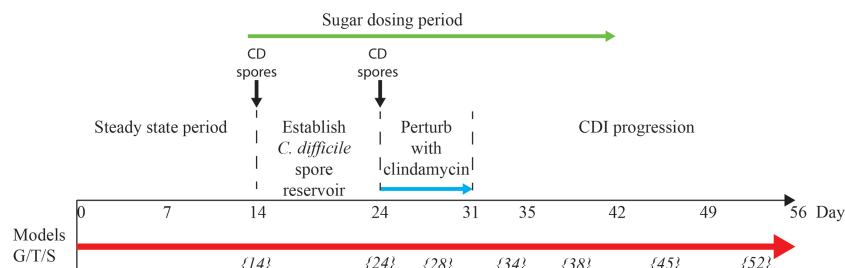


FIGURE 1 | Schematic timeline of the *in vitro* triple vessel chemostat gut model and experimental design for each model. *C. difficile* spores (black lines) were instilled and commencement of sugar regimen [either trehalose (T), glucose (G) or saline (S) (green arrow)] before addition of antibiotics (blue arrow). Microbial populations were monitored post antibiotic for recovery and induction of CDI. Numbers in italics brackets denotes the day that samples for DNA extraction were taken.

these agents have progressed to Phase III clinical trials. A recent publication detailing efficacy of extended duration fidaxomicin therapy (Chilton et al., 2015) led to the current Phase IIIB/IV trial investigating such dosing regimens in the clinic. In fact, data from gut model studies (Baines et al., 2005; Chilton et al., 2012; Baines et al., 2013) have informed UK national antibiotic prescribing guidelines (Public Health England, 2016). Using this *in vitro* model, we investigated the effects of trehalose on the colonic microbiota and progression of simulated CDI.

MATERIALS AND METHODS

Gut Model Set Up

Three triple-stage *in vitro* gut models were run in parallel as previously described (Moura et al., 2019). Briefly, each model consists of three chemostat vessels arranged in a weir cascade system, top-fed with a complex growth medium at a controlled rate ($D=0.015\text{ h}^{-1}$). All three vessels were continuously stirred, anaerobically maintained at 37°C and regulated to reflect *in vivo* intestinal conditions. The three vessels are representative of the colon, reflecting increased pH and decreased nutrient availability from the proximal colon (vessel 1, pH 5.5 ± 0.2), through the medial colon (vessel 2, pH 6.2 ± 0.2) to the distal colon (vessel 3, pH 6.8 ± 0.2). A faecal slurry (10% w/v) was made by diluting pooled human faeces from healthy elderly volunteers ($n = 5$; >59 years of age; CDI negative; no prior three-month history of antibiotic exposure) with pre-reduced PBS. Donors over the age of 59 were used to represent the at-risk group for developing CDI. This slurry, approximately 500 ml per model, was used to seed the vessels for each gut model at the start of the experiment.

Experimental Timeline

For each model, the microbial populations were allowed to equilibrate for two weeks to reach ‘steady state’ without intervention; consistent stable microbial recoveries over 5 days from all microbial populations tested was used to determine ‘steady state’. A single one ml aliquot of *C. difficile* RT027 strain 210 spores (approximately 10^7 cfu/ml) were inoculated into vessel 1 of each model and sugar supplementation commenced (**Figure 1**). Models were dosed with either glucose ($n=1$ model; model G; 1120 mM dosed thrice daily for 35 days), trehalose ($n=1$ model; model T; 560 mM thrice daily for 35 days), or phosphate buffered saline ($n=1$ model; model S; thrice daily for 35 days) (**Figure 1** – green arrow). The dosing regimens were inoculated in vessel 1, and sufficient to achieve final trehalose and glucose concentrations in vessel 1 of each model of 10 mM and 20 mM, respectively, i.e. consistent with levels observed in humans consuming trehalose (Abbott and Chen; Food Standards Australia New Zealand (FSANZ), 2003). A second dose of *C. difficile* strain 210 spores were inoculated as previously described, followed by a clindamycin regimen (33.9 mg/l four times daily for seven days) to induce simulated CDI (Chilton et al., 2014). The first *C. difficile* spore dose was added to ensure that the microbial populations within the model had

equilibrated and were able to prevent *C. difficile* spore germination; an effect called colonisation resistance. This ensured that the effects of any downstream manipulations of the microbiota were due to those manipulations rather than incomplete colonisation resistance.

Preparation of Ribotype-027 *C. difficile* Strain 210 Spores

Similar to other strains of ribotype-027, *C. difficile* 210 strain has a mutated *treR* repressor gene, as reported in (Collins et al., 2018a). *C. difficile* spores for gut model inoculation were prepared as previously described (Buckley et al., 2011). Briefly, *C. difficile* 210 was grown in BHI broth anaerobically at 37°C for six days and removed from the incubator and incubated aerobically at room temperature overnight to further induce sporulation. Growth was harvested by centrifugation and incubated with PBS supplemented with 10 mg/ml lysozyme at 37°C overnight. Samples were separated using a sucrose gradient and spores were treated with PBS supplemented with 20 ng/ml protease K and 200 nM EDTA. Spores were separated using a sucrose gradient and washed with PBS twice before a final resuspension in 30 ml. These were enumerated and diluted to approximately 1×10^7 spores/ml for use in the models.

Bacterial Enumeration Using Selective Agars

Vessel 3 of models T, S and G was sampled daily for culture profiling of total bacteria, lactose-fermenting Enterobacteriaceae, *Clostridium* spp., *Lactobacillus* spp., *Bifidobacterium* spp., *Enterococcus* spp., and *Bacteroides* spp., and *C. difficile* populations as described in **Supplementary Methods** and **Supplementary Table 4**. Colonies from these plates were identified to a species level by MALDI-TOF analysis.

Cytotoxin Assay

A VERO cell-based assay was used to approximate the level of toxin present in the gut model. This assay is a semi-quantitative measure of toxin activity within the gut models as many factors can affect the action of the toxin, e.g. protein levels, which were not normalised across each time point & sample. Samples from vessels 1, 2 & 3 were centrifuged and stored at 4°C before testing. Samples were serially diluted 1:10 and co-incubated with a confluent monolayer of VERO cells and incubated for 48 hr at 37°C, 5% CO₂. Toxin positivity was indicated by >50% cell rounding, while the confluent cell monolayer was unaffected in toxin negative samples. Presence of *C. difficile* toxin was confirmed by neutralisation of neat sample with *C. sordellii* antitoxin.

Antibiotic Bioassay

The concentration of clindamycin in each vessel was determined by bioassays as previously described (Chilton et al., 2014). Briefly, indicator organism *Kocuria rhizophila* (ATCC 9341) was inoculated into Wilkins-Chalgren agar and aseptically transferred into 245 x 245 mm agar plates. These plates were allowed to set, and nine mm wells were made using a cork borer. A calibration series of the antibiotic was added to each plate and

samples loaded into the wells. Plates were incubated overnight, aerobically at 37°C. Zone diameters were measured using callipers and concentration curves plotted from squared zone diameters and unknown concentrations from vessel supernatants determined. Assays were performed in triplicate.

Trehalose and Glucose Concentration

Daily gut model samples from all vessels of each model were assessed by ion chromatography for trehalose and glucose concentrations. Samples were tested in a blind fashion. Gut model samples were centrifuged at 15,000 rpm for 10 mins, and the supernatant was further centrifuged using millipore centrifugal filter units with a 50 kDa and 3 kDa cut off to remove proteins and bigger macromolecules. Samples were diluted 1:10 in ultrapure water and analysed by ion chromatography. 25 µl of sample was injected on a Dionex ICS-5000 plus ion chromatography system (Thermo fisher Scientific, USA). The separation was carried out on a Dionex CarboPac PA1 Analytical Column (4 x 250 mm) with a Dionex CarboPac PA1 Guard Column (4 x 50 mm). The column temperature was set at 30°C. Elution was performed using three elutants; A: ultrapure water, B: 300 mM sodium hydroxide and C: 300 mM sodium hydroxide with 1500 mM sodium acetate, with a flow rate of one ml/min. The linear gradient condition is shown in **Supplementary Table 5**. The analytes were detected by using an electrochemical detector.

DNA Extraction, Bacterial 16S rRNA Library Preparation and Sequencing

The bacterial 16S rRNA sampling regimen from vessel 3 of all three models are shown in **Figure 1**. Samples were taken prior to the first sugar dose, first clindamycin dose, in the middle of clindamycin dosing, 2 days after last clindamycin dose, i.e. after washout of clindamycin from the system, and weekly thereafter. Four one ml aliquots, representing four technical replicates, from vessel 3 of each model were pelleted, the supernatant discarded, and the DNA extracted from the pellet using FastDNA™ SPIN kit for soil (MP Biomedicals™) following manufacturers' instructions. DNA was stored at -80°C until used for downstream analysis. DNA quality and double-stranded quantities were determined using the picogreen absorption method. Bacterial 16S rRNA V4 fragments were PCR amplified using NEBNext Q5 Hot Start HiFi PCR master mix (NEB, U.K.) with universal 16S rRNA V4 primers [564F (TCGTCGCGCAGCGTCAGATGTGTATA>AGAGACAG-AYTGGGYDTAAAGNG) and 806R (GTCTCGTGGGCTCGGAGATGTGTATAAGAGACAG-TACNVGGGTATCTAATCC)] with Illumina adaptor sequence overhangs included using the PCR cycle [denaturation (95°C x3 min for 1 cycle), amplification (95°C x30 sec, 50°C x30 sec, 72°C x30 sec, for 28 cycles) and final elongation (72°C x5 min for 1 cycle)]. PCR products were cleaned using AxyPrep Magnetic beads (Axygen, U.K.) and the 16S rRNA fragments checked using gel electrophoresis on an Agilent 2200 TapeStation system (Agilent Genomics, U.K.) before running a PCR for addition of the index sequences [denaturation (95°C x3 min for 1 cycle), amplification (95°C x30 sec, 55°C x30 sec, 72°C x30 sec, for 8 cycles) and final elongation (72°C x5 min for 1 cycle)]. The fragments were cleaned,

quantified (as before), normalised and samples sequenced using MiSeq sequencer (Illumina) with 250 bp paired-end reads. Library preparation and sequencing was done at the University of Leeds sequencing facility.

Taxonomic Analysis on 16S rRNA Gene Sequences

Demultiplexed FASTQ files of 16S rRNA sequences were trimmed of adapter sequences using cutadapt (Martin, 2011), and samples were filtered based on the number of reads across all samples to provide similar coverage. We followed the standard operating procedure from the MOTHUR package (v.1.41.3) (Schloss et al., 2009). The paired reads were joined together and assembled into the contigs, and quality controlled based on the parameters such as maxambig=0, minlength=177 and maxlength=237. Unique sequences were aligned against a tailor-made reference generated from SILVA SEED database (version 132) and further filtered according to their start and end positions in the alignments. In order to reduce the possible redundancy to a minimum, the identical and very similar sequences (within 2bp mismatch) were merged. The chimeric sequences were discarded based on the built-in VSEARCH method (Rognes et al., 2016). OTUs (operational taxonomic units) were identified by clustering (0.5 UniFrac distance) the sequences and were assigned the consensus taxonomy information with label=0.03. Low abundant reads (<50 reads per sample, which accounted for <0.04% of the total reads) were removed before further analysis; however, this precludes the contribution of low abundance taxonomic families in our analysis whilst ensuring accuracy from sequencing artifact. Taxonomic analysis is represented as mean percent abundance from four technical replicates. To determine if a microbial community was differentially abundant between the technical replicates of the three models on a given day a differential abundance analysis was performed and a microbial community was considered significantly different when the false discovery rate (FDR) p value was ≤ 0.01 and a $-1.5 \leq \text{Log}_2$ fold change ≥ 1.5 of the populations in model T in comparison with models G and S was observed. The same cut off values were used to determine the difference in abundance of the microbial populations of the slurry compared to the models T, G, and S at day 14. For the calculations of bacterial diversity, Shannon diversity index was computed for all samples and the distance matrix based on the Bray-Curtis approach was used for Principal Coordinates (PCoA) analysis and visualization for each group of samples, based on four technical replicates. A Mann-Whitney U test was performed to determine statistical significance between the pre-clindamycin Shannon diversity index reference and the other timepoints for each model.

Functional Analysis of the Microbiota

All samples collected from model T throughout the experiment (time points shown in **Figure 1**) and samples from model S and G on day 38 (1-week post clindamycin), were selected for shotgun metagenome sequencing. Four technical replicates were investigated for each time point. Extracted DNA was

diluted to 500 ng and sheared to 200–300 bp using an E220 focused ultrasonicator (Covaris, U.K.). NEBNext Ultra DNA Library prep kit for Illumina was used for adaptor ligation and to PCR enrichment following manufacturer's instructions. Libraries were sequenced using Illumina HiSeq 3000 sequencer (University of Leeds). FASTX-Toolkit (version 0.0.13) was used to trim the first 10 bp from the sequence reads. MEGAN UE (ultimate edition v6.18.0) was used to functionally annotate and compare the sequencing reads using inbuilt programme tools (Huson et al., 2016). Briefly, paired-end reads were aligned on to NCBI-nr database (version 14.12.19; nr.gr size: 52.5 Gb) using DIAMOND (Buchfink et al., 2014) and Meganizer was used to perform functional analysis of the DIAMOND input files using either an up-to-date representation of KEGG or Pfam-A database (version 32). KEGG orthologous groups (Ko groups) were mapped to enzymes that appear in metabolic pathways. Functional analysis using KEGG assigned 39–43% of the total reads to a Ko group. An abundance table of functional categories for each sample was generated and a differential proportion-based abundance analysis, based on z test (Kal et al., 1999), was performed. A functional annotation was considered significantly different when the false discovery rate (FDR) p value was ≤ 0.05 and a $-1.5 \leq \text{Log}_2$ fold change ≥ 1.5 of the populations, based on z-score, in model T in comparison with models G and S. Variations in Ko groups (metabolic pathways and surface components) were considered significant when the fold-change of at least 80% of the genetic components in that pathway were either more or less abundant (as described above). The abundance of trehalase-specific Pfam terms, trehalase (clan 0059) and trehalose phosphatase (clan 0137), throughout all timepoints of model T were compared, and fold change abundance calculated.

Taxonomic Profiling of Whole Genome Sequences

Taxonomic profiling from the whole genome paired sequences generated above was performed using CLC Genomics Workbench (version 12.0.3), with the CLC Microbial Genomics Module (version 4.8). Trimmed sequences were imported into the CLC software and each sequence read individually mapped to the fully curated (as of June 2019) microbial reference database, based on selected references from GenBank and RefSeq, using the default settings in the *Taxonomic Profiling* tool. Abundance tables were merged, and the *Differential Abundance Analysis* tool used to determine the abundance differential in taxa, compared to model T, based on a Log_2 fold-change < -2 or > 2 and a Wald test false discovery rate (FDR) p value < 0.001 .

RESULTS

Reconstitution of the Human Microbiota in the Gut Model

Each triple-staged gut model is seeded with a faecal slurry made using the pooled faecal matter from five healthy donors to capture a diverse representation of the human microbial

populations (**Figure 1**). Firstly, we sought to characterise the microbial diversity captured from this slurry in each gut model. The donors used in this study showed distinct microbial profiles to each other (**Supplementary Table 1**), except for donors E and C, which clustered together, indicating similar microbiota profiles. Similarly, the faecal slurry used clustered distinctly from each donor but nested amongst the donors, suggesting the slurry contains the overall diversity from the donors; indeed, the slurry contained 36 bacterial families, more than each individual donor (**Figure 2A**). As determined by bacterial taxonomic analysis by 16S rRNA sequencing, the slurry was found to contain bacterial family members that were unique to a single donor, for example *Eubacteriaceae* and *Muribaculaceae* were only present in Donor C and the slurry (**Supplementary Table 1**). Once the microbial populations had stabilised in the three models, the predominant bacterial families were represented at similar levels to the slurry (**Figures 2B, C**), although some differences were observed. Compared with the faecal slurry, *Bifidobacteriaceae* abundance increased and *Clostridiaceae* abundance decreased in all models at steady state, whereas *Coriobacteriaceae* showed increased abundance in models G and S and *Enterococcaceae* abundance increased in model T (**Figure 2C**). However, *Bifidobacteriaceae* did decrease in all models one week later, which was confirmed by direct enumeration.

The Changing Bioavailability of Trehalose

The trehalose dosing regimen in model T was designed to mimic the average trehalose content from meals consumed thrice daily by an adult, which can vary amongst adults and different countries (Abbott and Chen; Food Standards Australia New Zealand (FSANZ), 2003). Trehalose was undetected in the saline (control) model S and was only detected periodically in vessel 1 (proximal colon) of the model G dosed with glucose (0.01 mM), whereas trehalose supplementation in model T increased detectable trehalose concentrations, peaking at 8.1 mM in vessel 1 of model T prior to addition of antibiotics (**Figure 3**). Trehalose was largely undetectable in vessels 2 (medial colon, pH 6.2 ± 0.2) and 3 (distal colon, pH 6.8 ± 0.2) of each model, although trehalose was observed in vessel 2 up to three days after commencing dosing, peaking at 4.3 mM (**Supplementary Table 2**). As trehalose can be catabolised into two glucose molecules, model G was dosed with glucose at double the concentration of trehalose to determine if any effects of trehalose on the microbial populations was not due to the increased glucose availability (**Figure 3A**). Prior to antibiotic dosing, commencement of the glucose dosing regimen was associated with a peak glucose concentration of 16.1 mM in model G, compared with 0.1 mM and 0.007 mM in models T and S, respectively.

Addition of clindamycin induced microbial dysbiosis in model T, which correlated with increased luminal concentrations of trehalose in all vessels (**Supplementary Table 2**); peak trehalose detection in vessels 1, 2 and 3 were 13.3, 6.7 and 2.5 mM, respectively (**Figure 3**). However, luminal concentrations of trehalose reduced to undetectable levels in vessels 2 and 3, and to approximately 2.1 mM in vessel 1, on the last day of clindamycin instillation (day 31). A similar pattern of increased trehalose bioavailability during clindamycin instillation, albeit at

much lower levels, was observed in models G (vessels 1-2) and S (vessel 1-3), which, although were not dosed with trehalose throughout the experiment, had trehalose in the growth media. During clindamycin instillation, we detected greater bioavailability of glucose in all models at day 26, particularly in vessel 1 (**Figure 3**). Model G had the highest concentration, peaking at 28.3 mM and concentrations in models T and S peaked at 1.6 and 1.8, respectively. The initial reduction in microbial diversity caused by clindamycin, and the increased trehalose bioavailability, resulted in an increased abundance of microbial genomes harbouring Pfam domains for trehalose metabolism [trehalase (clan 0059) and trehalose phosphatase (clan 0137)]; these domains increased 4.6- and 4.4-fold, respectively, compared with the abundance of these domains pre-trehalose levels (**Table 1**). One week after clindamycin, the abundance of these Pfam domains reduced to levels similar to pre-clindamycin.

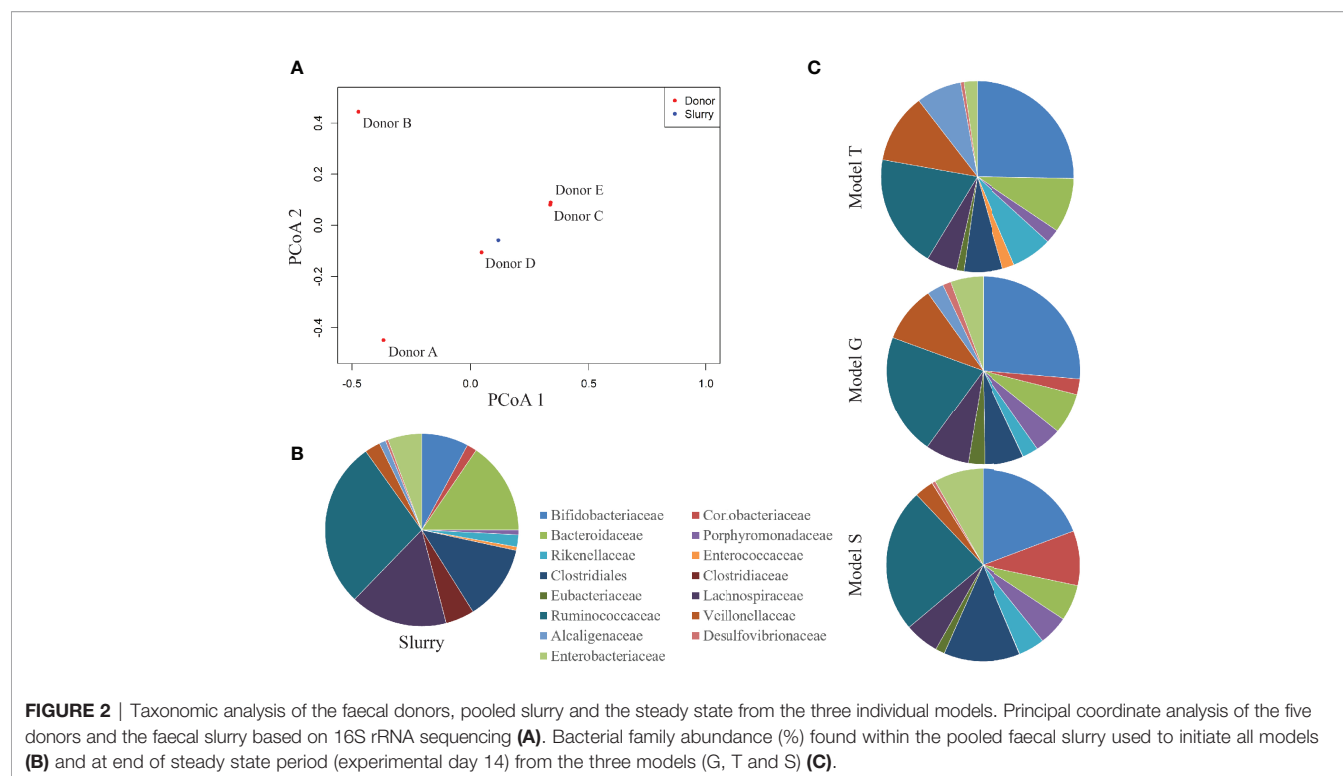
Remodelling of the Microbiota in Response to Trehalose

Changes in the bacterial composition of the three models (T, G, and S) were monitored by 16S rRNA sequencing and taxonomic analysis (timepoints shown in **Figure 1**) and direct enumeration of selected bacterial populations (daily monitoring), to determine how trehalose dosing affected the gut microbiota, compared to glucose or saline. Prior to clindamycin exposure, the microbial populations largely remained stable in the control (saline dosed) model (**Figure 4**), whilst trehalose exposure in model T was specifically associated with an increase in abundance of *Bacteroides uniformis* to almost 3% of the total bacterial

populations, identified by shotgun metagenomic sequencing. This increase was confirmed by selective enumeration of *Bacteroides* spp. and species identification by MALDI-TOF analysis. Similar abundance increases were observed in other microbial populations specifically from model T, *Coprococcus* spp. (*C. catus*, *C. comes* and *C. eutactus*), *Blautia* spp. (*B. producta* and *B. obeum*), *Veillonella dispar* and *Lactobacillaceae* (*L. fermentum* and *L. johnsonii*) (**Figures 4A, B**). Similarly, the enumerated recoveries of *Lactobacillus* spp. in model T showed a 1.2 log₁₀ cfu/ml increase in response to trehalose instillation (**Supplementary Figure 1**). However, the changes in microbiota did not result in germination of *C. difficile* spores prior to addition of clindamycin. This increase in certain bacterial populations were mirrored by an increase in the number of Pfam domains associated with trehalose metabolism in model T. Trehalase- (PF01204/EC:3.2.1.28) and trehalose phosphatase-related (PF02358/EC:3.1.3.12) Pfam domains increased 3.6- and 1.4-fold, respectively, in abundance upon commencement of trehalose dosing compared with pre-trehalose levels (**Table 1**). The increased abundance of Pfam domains associated with trehalose metabolism correlated with an increase abundance of those bacterial species with known trehalose metabolising capabilities.

Clindamycin Reduced the Microbial Diversity

CDI induction is reliant on microbial disruption, typically through antibiotic exposure. As we observed sugar-mediated microbiota reconfiguration in our models, we sought to determine how



clindamycin induced (Chilton et al., 2014) disruption affected the bioavailability of trehalose that could subsequently be utilised by *C. difficile*. Clindamycin levels in vessel 1 peaked at 93.1, 142.5 and 127.1 mg/L, in models G, T and S, respectively. Upon clindamycin instillation, bacterial diversity significantly decreased ($p < 0.001$) from pre-clindamycin levels across all the models to a similar extent (Figure 4 line graphs); however, by three weeks after cessation of clindamycin instillation, bacterial diversity had not recovered to pre-clindamycin levels. This decreased diversity in all models was characterised by significant

($p \leq 0.01$) reductions to *Bifidobacteriaceae*, *Bacteroidaceae* (*B. gallinarum* and *B. intestinalis*), *Lachnospiraceae*, *Alcaligenaceae*, *Porphyromonadaceae* and *Veillonellaceae* populations, either during (intra-) or just after (four days post) clindamycin (Figure 4 bar graphs). However, *Enterobacteriaceae* (specifically *E. coli* and *K. pneumoniae*, as determined by MALDI-TOF analysis) and *Enterococcaceae* increased in relative abundance either during or just after antibiotic withdrawal, with an increase in bacterial populations confirmed by direct culture using selective agars (*Enterobacteriaceae* increased 2.4, 2.3, and 2.5 \log_{10} cfu/ml;

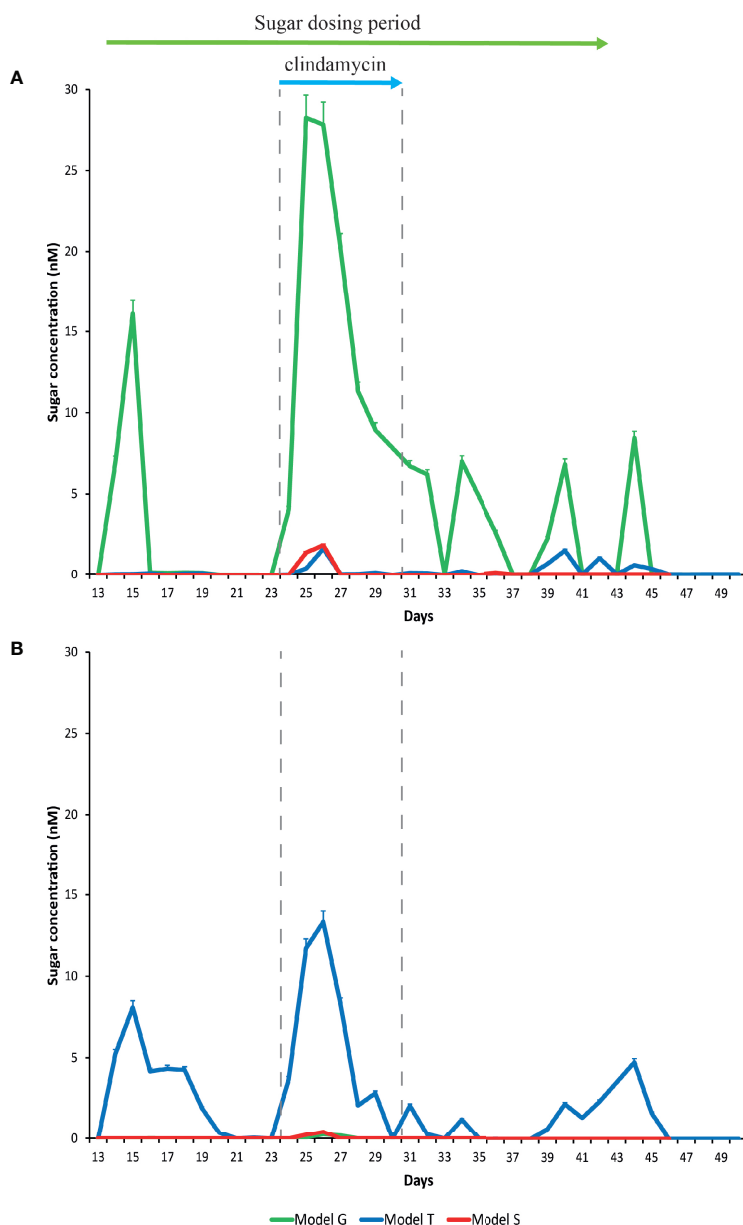


FIGURE 3 | Detection of glucose (A) and trehalose (B) in the gut models. Sugar concentrations from model T (blue lines), G (green lines), and S (red lines) were detected by ion chromatography. Results are shown as mean \pm S.D. of three technical replicates. Sugar duration and clindamycin dosing are indicated by the top green and blue arrows, respectively.

TABLE 1 | Abundance of trehalose specific Pfam domains in model T.

Pfam domain	Experimental period			
	Steady state	Pre-clindamycin	During clindamycin	1-week post clindamycin
Trehalose phosphatase	463	1673	7321	1110
Trehalase	4908	6871	31494	6871

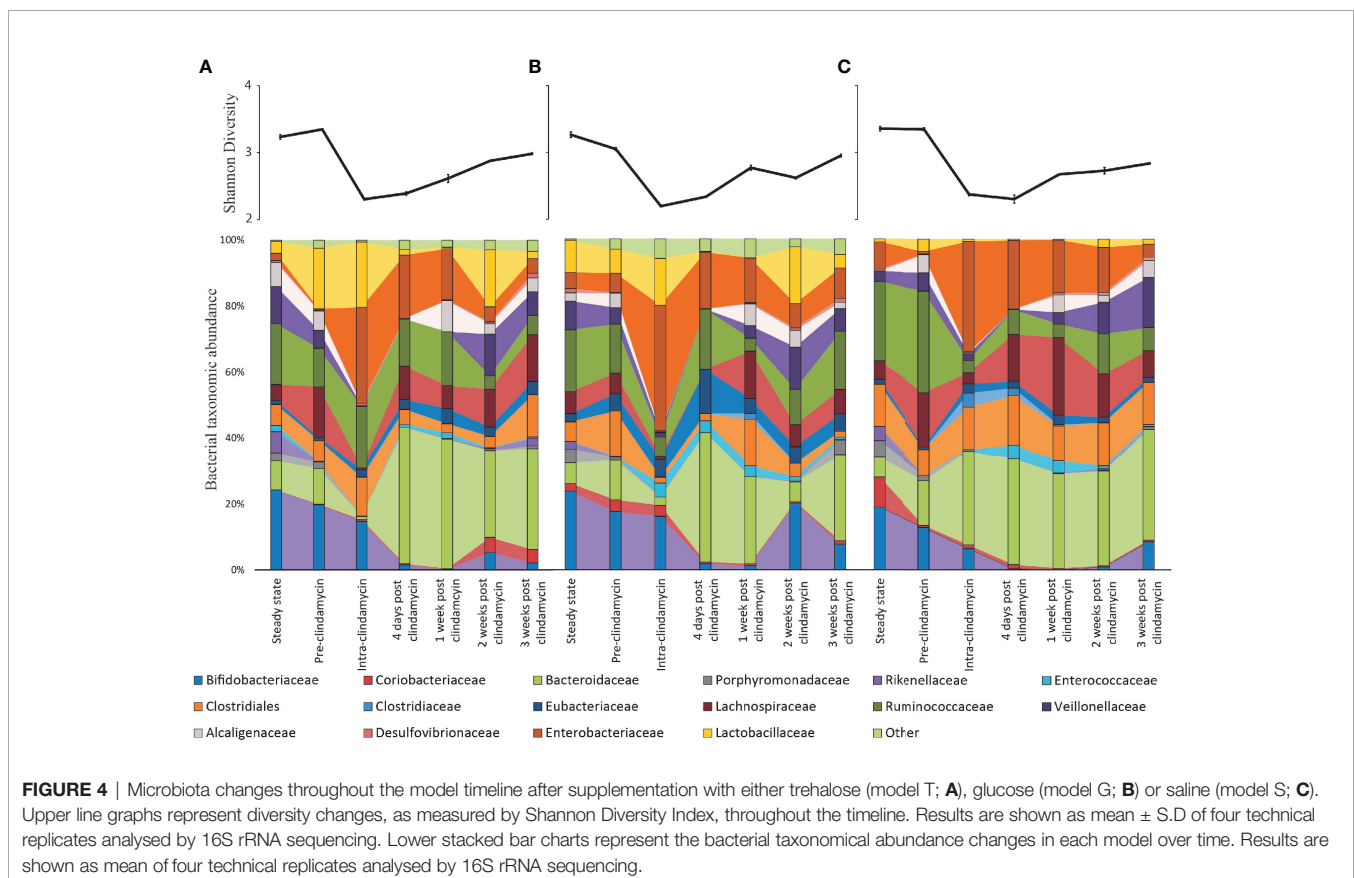
Enterococcus increased 1.8, 2.2, and 2.3 log₁₀ cfu/ml, in models G, S and T, respectively, during this time) (**Supplementary Figure 1**). This pattern of clindamycin-induced microbial dysbiosis is synonymous with induction of CDI in our *in vitro* gut model, as previously seen (Chilton et al., 2014; Eyre et al., 2019).

Trehalose Induced Microbiome Changes Prevents Simulated CDI

We hypothesized that the differential pattern of clindamycin-induced microbiota disruption, seen between the three models, and the subsequent microbial recoveries would affect the progression of simulated CDI. Prior to clindamycin instillation, in both the saline supplemented model S (**Figure 5A**), and the glucose supplemented model G (**Figure 5B**), *C. difficile* populations remained in the form of spores from its addition to the models on day 14. However, *C. difficile* germination and

outgrowth was detected one-week post clindamycin (day 38) with toxin detected from two days later until the end of the experiment, which is consistent with simulated CDI. Similarly, in the trehalose supplemented model, *C. difficile* spores remained quiescent until day 38, where we detected germination and limited outgrowth but, crucially, no toxin was detected throughout the experiment and the *C. difficile* levels decreased four days later to those consistent with the recovery of *C. difficile* spores (**Figure 5C**). We have previously reported this phenotypic observation in our gut model (Eyre et al., 2019). Thus, we further investigated the comparative microbiota differences and metabolic abundances on this day between models S/G and model T related to *C. difficile* proliferation and onset of simulated CDI.

Metagenomic analysis of the microbiota between models S/G and model T on day 38 highlighted 25 significant differentially abundant bacterial communities between model T (no simulated CDI) and models S and G (induced simulated CDI) (**Table 2**). *Fingoldia magna*, *Blautia obeum*, *Faecalibacterium prausnitzii*, *Dorea formicigenerans*, *Lactobacillus rhamnosus* and *Oscillospira ruminantium* were significantly ($p < 0.001$) more abundant in model T compared with models G and S, whereas, *Phascolarctobacterium* spp., *Klebsiella* spp. (*K. pneumoniae* and *K. aerogenes*), *E. faecalis* and several *Clostridium* spp. [*C. symbiosum*, *C. clostridioforme*, *C. citroniae* and *Hungatella hathewayi* (formally known as *C. hathewayi*)] were significantly less abundant in model



T. The increased abundance of *Lactobacillus* spp. in model T at day 38 compared with models S and G, was confirmed by direct enumeration, where *Lactobacillus* spp. levels in model T were 5.9 log₁₀ cfu/ml, compared with 3.8 and 3.2 log₁₀ cfu/ml for models S and G, respectively (**Supplementary Figure 1**). Similarly, at day 38, the recovery of *Clostridium* spp. and *Enterobacteriaceae* were higher in models S and G, compared with model T (**Supplementary Figure 1**). Analysing the metagenome function showed that components of the V/A-type ATPase were more abundant in models G and S, a conserved ATPase found only in *Enterococcus* spp (Murata et al., 2005). Additionally, the high levels of *Clostridium*

spp. (including former *Clostridium* species) found in models G and S was reflected in the increased abundance of those genetic elements involved in the sporulation cascade (*spo* genes).

Long-term supplementation of trehalose was associated with enhanced recovery of the Ruminococcaceae family, particularly the *Oscillospira*, *Erysipelotrichaceae* and *Anaeroplasmataceae* genera, 3-weeks post-clindamycin (**Figure 4A**). Inversely, *Bifidobacteriaceae* abundance in model T took longer to recover than the other models, where abundance remained at approximately 2% compared with 7.2-7.6% abundance observed in the other models. This was reflected in the bacterial recoveries

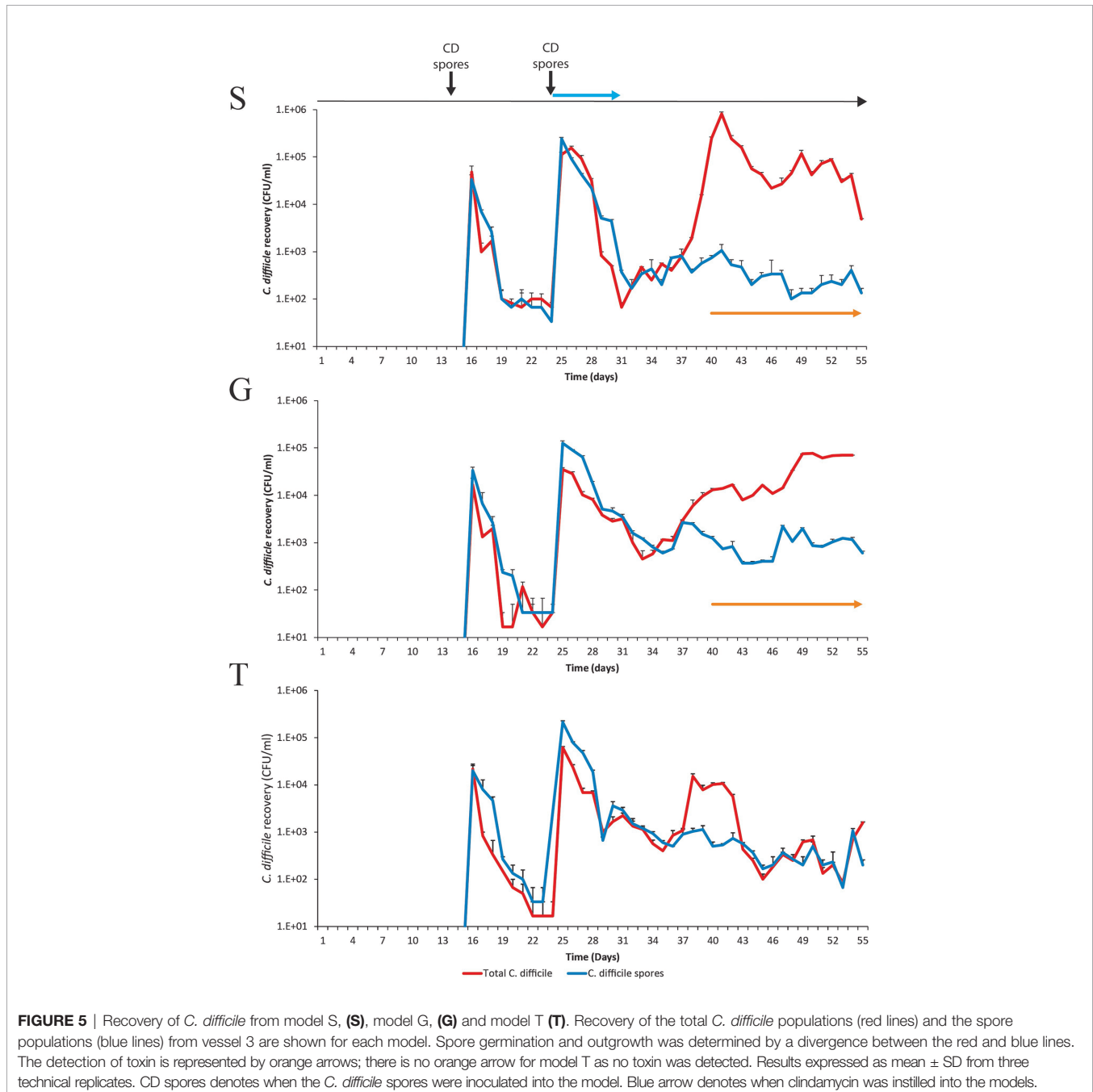


TABLE 2 | Differential abundance analysis of model T, compared to models G and S, at day 38.

Population name ^a	Log ₂ fold change ^b	
	vs. Model G	vs. Model S
s_ <i>Bacteroides uniformis</i>	-15.24	-15.14
s_ <i>Faecalibacterium prausnitzii</i>	-15.07	-14.97
s_ <i>Fingoldia magna</i>	-14.92	-14.82
s_ <i>Blautia obeum</i>	-14.81	-14.71
s_ <i>Dorea formicigenerans</i>	-14.57	-14.47
s_ <i>Lactobacillus rhamnosus</i>	-12.35	-12.25
s_ <i>Oscillibacter ruminantium</i>	-2.61	-19.61
s_ <i>Hungatella hathewayi</i>	18.22	16.8
s_ <i>Clostridium symbiosum</i>	17.12	18.08
s_ <i>Klebsiella aerogenes</i>	17.05	16.72
s_ <i>Blautia producta</i>	15.51	16.06
s_ <i>Clostridium clostridioforme</i>	15.30	16.43
s_ <i>Enterococcus faecalis</i>	3.4	3.59
s_ <i>Klebsiella pneumoniae</i>	3.18	2.27
s_ <i>Clostridium citroniae</i>	3.05	2.57
g_ <i>Pantoea</i>	-14.91	-14.81
g_ <i>Erysipelatoclostridium</i>	-14.83	-14.73
g_ <i>Cronobacter</i>	-14.55	-14.45
g_ <i>Eubacterium</i>	-14.45	-14.36
g_ <i>Xanthomonas</i>	-14.38	-14.28
g_ <i>Paraprevotella</i>	-14.34	-14.24
g_ <i>Ochrobactrum</i>	-12.52	-12.42
g_ <i>Phascolarctobacterium</i>	20.06	19.12
g_ <i>Clostridium</i>	15.98	16.47
f_ <i>Peptoniphilaceae</i>	-12.44	-12.34

^aTaxonomic level of microbial populations from whole genome sequencing data. s_ species, g_ genus or f_ family.

^bLog₂ fold change compared with model T, i.e. a positive number (red) indicates microbial population was significantly (FDR $p \leq 0.01$) less abundant in model T compared with models G and S, whilst a negative number (green) indicates microbial population was significantly (FDR $p \leq 0.01$) more abundant in model T.

where *Bifidobacterium* spp. levels recovered by days 13 and 9 (after clindamycin instillation) in models S and G, respectively, and day 19 in model T.

Functional Microbiome Changes Associated With CDI

In order to identify the microbial pathways active during CDI induction, a functional analysis of KEGG metabolic pathways was performed between model T, supplemented with trehalose, and models G and S, supplemented with glucose and saline (**Supplementary Table 3**). Comparison of the functional metabolic pathways between models was performed on day 38 (one-week post clindamycin), when CDI was detected in models G and S but not in model T. Model T showed differences to the metabolic landscape and cell surface components of the microbial species present, in comparison to models G and S (**Supplementary Table 4**). Whilst the abundance of genes involved in glucose/gluconeogenesis and the pentose phosphate pathway were similar across the models, other metabolic pathways that produced the central metabolites glyceraldehyde-3 phosphate (G3P) and D-glucose from different sugar sources, such lactose, galactose and *myo*-inositol, were more abundant in models G and S, whereas genes involved in trehalose metabolism were more abundant in

model T (**Figure 6A**). Interestingly, several pathways to produce amino acids (glutamine and glutamate) or amino acid precursors (chorismate and D-ribose-1,5P) were abundant in models G and S. Alongside the increased abundance of the intracellular stress molecule guanosine pentaphosphate (ppGpp), this could indicate a depleted pool of free amino acids (**Supplementary Figure 2**). In contrast, we detected an increased abundance of genetic components involved in the conversion of L-glutamine to the short chain fatty acid, butyrate (**Figure 6A**).

Differential abundance analysis of the shotgun metagenome sequences from these models suggests that the microbial species could have distinctive cell surface arrangements. In all three models, genetic elements associated with biofilm formation were present; however, these genetic elements were different between the models. Model T had increased abundance of genes involved with curli biosynthesis, important in Enterobacteriaceae biofilm formation, whereas, the genes involved in production of extracellular matrix (PGA) were more abundant in models G and S (**Figure 6B**). The presence of classical virulence factors were also different; genetic elements associated with siderophore production (yersiniabactin and bacitracin) and type 4 secretion systems (T4SS) were more abundant in models G and S, whilst genes involved in the production of polysaccharide capsule were less abundant. Additionally, ABC transporter systems were different between the models; sugar transport systems, for ribose, lactose, arabinogalactan and cellobiose, were more abundant in models G and S, whilst the general L-amino acid transporter was more abundant in model T (**Figure 6B**).

In summary, the colonic microbiota remodelled to better utilise the supplemented trehalose, and this was associated with an increase in the abundance of trehalose-metabolising genes. This lack of bioavailable trehalose negated the ability of a *C. difficile* strain with enhanced trehalose metabolism to colonise and cause fulfiment CDI, despite creating a growth niche with clindamycin and continuous trehalose supplementation, unlike glucose and saline supplementation.

DISCUSSION

The consumption of trehalose has been proposed to contribute to the emergence and virulence of CDI outbreaks, specifically in those RTs harbouring genetic trehalose metabolism variants (Collins et al., 2018a; Collins et al., 2018b). Some RT lineages, such as RT027, have a mutated repressor, *treR*, gene, whilst others, such as RT078, have acquired a putative *ptsT* transport system, which gives them a competitive advantage during pathogenesis (Collins et al., 2018b). However, we and others have reported that these genetic variants are common in multiple *C. difficile* lineages not associated with clinical outbreaks and there was no association between trehalose metabolism variant and clinical outcome (Eyre et al., 2019; Saund et al., 2020). Here we describe the effects of trehalose supplementation on the human microbiota and how the recovery of the microbiota can affect simulated CDI, using a clinically reflective gut model. This model has been used to successfully predict trial outcome at

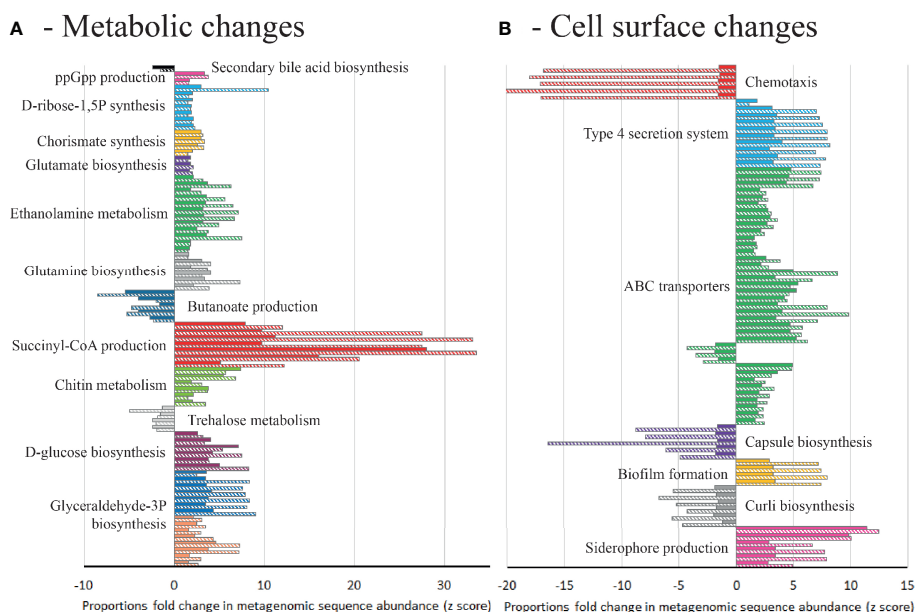


FIGURE 6 | Differential abundance analysis (fold-change) of metabolic pathways in model T compared to models G (solid bars) and S (hatched bars) at day 38, based on metagenomics analysis. Abundance bars highlight the KEGG metabolic pathways (A) or KEGG cell surface components (B) that are significantly ($p < 0.05$) more abundant (> 1.5 fold-change) or less abundant (> 1.5 fold-change) in model T. Pathways or components were only included where 80% of the genetic elements in that pathway/component showed an increased or decreased abundance from technical replicates of model T compared to both models G and S (Supplementary Table 4).

various stages of pre-clinical and clinical therapeutic development. However, due to the limited number of biological replicates ($n=2$), our conclusions are presented as preliminary findings. Numerous reports have highlighted key microbiota differences between humans and mice (Ley et al., 2005; Nguyen et al., 2015), which is potentially important given the contribution of the microbiota towards colonisation resistance against CDI. Indeed, mice bred in captivity, on the same diet, have a similar microbiota (Hufeldt et al., 2010), which is far removed from the heterogeneity displayed within a human population, and could result in different clinical outcomes (Selber-hnativ et al., 2017). The major human microbial communities present in the donor faeces were represented in the faecal slurry used to seed each model, and we subsequently recaptured these communities in each of our human ‘gut models’. Three independent models were run in parallel, supplemented with either trehalose, glucose or saline. As trehalose can be metabolised into two glucose molecules, this experimental approach was used to delineate the effects of trehalose rather than its breakdown product.

Trehalose supplementation immediately increased the trehalose concentration in vessels 1 and 2; however, despite continued trehalose supplementation, the levels decreased to undetectable levels, suggesting microbial trehalose metabolism. This drop in trehalose concentration was specifically associated with an increased abundance of trehalose metabolising Pfam domains and a corresponding remodelling of the microbiota to

include higher abundances of *B. uniformis*, *B. producta* and *V. dispar*. Many strains of these bacterial species are known to harbour *treA*-like genes, a trehalose-6-phosphatase that metabolises trehalose into glucose and glucose-6-phosphate monomers (Rogosa, 1964; Whatmore et al., 1990; Liu et al., 2008). Trehalose metabolism appears not to be restricted to these bacterial species, indeed, the UniProt protein sequence repository suggests trehalose metabolising genes are ubiquitous amongst bacterial species (Bateman et al., 2017). Further evidence of the role of the intestinal microbiota to metabolise trehalose is shown during clindamycin exposure. Clindamycin is a broad-spectrum antibiotic that has previously been shown to induce CDI in our gut model (Chilton et al., 2014). Clindamycin instillation decreased the microbial diversity in all models, causing simulated intestinal dysbiosis, which correlated with increased bioavailability of trehalose. It would be interesting to see if this effect is replicated using other antibiotics associated with induction of CDI. The levels of trehalose returned to undetectable levels in vessels 2 and 3 prior to completion of the clindamycin regimen; these vessels simulate the medial and distal colon, which is most conducive for CDI (Freeman et al., 2003). We used a highly sensitive method to quantify trehalose/glucose concentrations, with a limit of detection at $0.5\mu\text{M}$. Collins et al. reported *C. difficile* trehalose metabolism variants that could utilise $50\mu\text{M}$ - 25mM concentrations of trehalose more efficiently, compared with wildtype trehalose metabolism variants (Collins et al., 2018a). We hypothesised that, although

C. difficile trehalose metabolism variants could have a competitive advantage over wildtype isolates, this competitive advantage is diminished in the presence of the human microbiota, as the intestinal microbiota is an important source of trehalose metabolism, potentially reducing the bioavailability of trehalose during CDI. However, the competitiveness of the human microbiota against *C. difficile* with respect to trehalose utilisation requires further study to determine mechanisms of competition under *in vivo* conditions. Further evidence for this is shown using degradation-resistant trehalose analogues, such as lactotrehalose, which show enhanced faecal bioavailability and, additionally, does not induce CDI in a mouse model (Zhang and DeBosch, 2020). The Ribotype 027 strain used in our studies possesses a *treR* mutation. It would be interesting to determine the competitiveness of a strain harbouring a putative *ptsT* transport system, which could provide a competitive trehalose metabolic advantage over the microbiota (Collins et al., 2018b).

Instillation of clindamycin did result in induction of simulated CDI in models supplemented with either glucose or saline; however, trehalose supplementation did not result in simulated CDI [(Eyre et al., 2019) and **Figure 5**]. Differential taxonomic abundance between model T and models G/S identified bacterial species that were either more (n=7) or less (n=8) abundant in model T; although these data are from one independent biological repeat of each condition. Of the bacterial species associated with protection against CDI, *B. uniformis* was the dominant *Bacteroides* species identified in model T (3% of total reads) and is capable of metabolising trehalose. Through metabolite cross-feeding, *B. uniformis* can support the growth of *F. prausnitzii* (Chung et al., 2016), and vice versa, which enhances the growth of both species. *F. prausnitzii* is known to produce butyrate and formate, which have been shown to reduce inflammation during infection (Fachi et al., 2019), but increased levels of *F. prausnitzii* were associated with recovery from CDI in patients and *in vivo* models (Khanna et al., 2016; Roychowdhury et al., 2018). Strains of *B. obeum* can also utilise trehalose, and crucially, have been shown to reduce virulence gene expression, through quorum sensing, during *Vibrio cholerae* infection (Hsiao et al., 2014); toxin synthesis by *C. difficile* can be regulated by different quorum sensing (Lee and Song, 2005; Darkoh et al., 2015). The metabolic interconnectivity between these microbial species could represent a consortium that competes for nutrients utilised by *C. difficile* after spore germination (as hypothesised in **Supplementary Figure 3**). Furthermore, the increased abundance of these bacterial species associated with CDI prevention in model T are less abundant in the faeces from CDI patients and have been attributed with protective effects in putative microbiome restoratives (Reeves et al., 2011; Petrof et al., 2013; Milani et al., 2016). Moreover, carbohydrate-induced microbiota outgrowth, and subsequent metabolic products, were associated with a decrease in *C. difficile* fitness (Hryckowian et al., 2018), similar to our *in vitro* findings. In our study we used the microbiota from healthy donors above the age of 59 as this age group has the highest risk of developing CDI. However, we know that microbiome composition is affected by age (Pasolli 2019), thus it would be interesting to determine if

donors from other age groups have a differing ability to metabolise trehalose. Aside from acting as a potential carbon source, intracellular trehalose has unique properties that could protect cells from the effects of antibiotics, such as a membrane osmoprotectant and a protein stabilising molecule (Elbein et al., 2003; Jain and Roy, 2009).

Interestingly, 4 different *Clostridium* spp. were associated with CDI induction in model's G/S. A similar observation was noted by Khanna et al. (2016) and Daquigan et al. (2017), where several *Clostridium* spp. were associated with increased *C. difficile* abundance in CDI and recurrent CDI patients. Additionally, Girinathan et al. showed the presence of *Clostridium sardiniense* enhanced CDI in an *in vivo* model of disease (Girinathan et al., 2020). Conversely, the authors observed that *C. bifermentans*, an amino acid fermenter, prevented CDI-induced death in an animal model of infection. The bioavailability of amino acids play a crucial role in *C. difficile* pathogenesis. Glycine is a potent germinator for *C. difficile* spores, and *C. difficile* utilises amino acids, particularly isoleucine and proline, during *in vitro* and *in vivo* growth as both a carbon source and an energy source, via Stickland reactions (Bouillaut et al., 2013; Hofmann et al., 2018; Battaglioli et al., 2018; Robinson et al., 2019). Microorganisms that compete for bioavailable amino acids, such as *C. bifermentans*, could prevent the rapid proliferation of *C. difficile* during CDI (Girinathan et al., 2020). Indeed, the CDI-linked functional profile of the microbiota favoured the production of amino acids (or amino acid precursors) from sugars, potentially due to a reduced pool of bioavailable amino acids after being used by *C. difficile* during pathogen expansion. This was mirrored in the functions of the cell surface ABC transporters where there was an increased abundance of sugar transporters in models G and S, potentially associated with *C. difficile* proliferation niche. The identified metabolic pathways and putative metabolic products associated with CDI induction in our gut models, namely G3P/D-ribose-5P/succinyl-CoA/inosine, have been shown to be utilised by *C. difficile* during *in vivo* growth in a murine model of infection (Jenior et al., 2017) and as CDI-associated metabolites in cohorts of CDI patients (Robinson et al., 2019). Other CDI-associated metabolites, such as ethanolamine and succinate, identified in this study have been confirmed as an important nutrient source (Ferreira et al., 2014; McDonald et al., 2018; Nawrocki et al., 2018).

By studying the effect of trehalose at a systems level, we outline plasticity of the human microbiome to adapt to utilise this carbon source, providing competition with *C. difficile*. The absence of enhanced CDI associated with trehalose in this model system, and the mechanisms explained, could help explain why clinical outcome was not associated with genetic markers for enhanced trehalose metabolism. Contrary to enhancing CDI, trehalose utilisation was preliminary linked with a consortium of cross-feeding microbial species that may be antagonistic to the growth of *C. difficile*, which can form the rationale for the basis of microbial therapies used for treating CDI infections (**Supplementary Figure 3**). Further *in vitro* and *in vivo* studies are required to confirm these preliminary data.

AUTHOR'S NOTE

Samples were analysed in a blind fashion; samples were labelled and randomised in such a way that the funders did not know what models/vessels/experimental phase the samples were.

DATA AVAILABILITY STATEMENT

Sequencing data associated with this manuscript has been deposited in the Sequence Read Archive (SRA), Bioproject PRJNA644077: Effect of trehalose on the human microbiota and the prevention of simulated *Clostridioides difficile* infection.

ETHICS STATEMENT

The collection and use of human faeces in our gut model has been approved by the School of Medicine Research Ethics Committee, University of Leeds (MREC 15-070 – Investigation of the Interplay between Commensal Intestinal Organisms and Pathogenic Bacteria). Participants were provided with a 'Participant Information Sheet' (PIS) detailing a lay summary of the *in vitro* gut model and the scientific work they were contributing to by providing a faecal donation. Within this PIS, it is explained that by providing the sample, the participant is giving informed consent for that sample to be used in the gut model.

REFERENCES

- Abbott, P. J., and Chen, J. *WHO Food Additives Series 46: Trehalose*. Available at: <http://www.inchem.org/documents/jecfa/jecmono/v46je05.htm>.
- Arguelles, J. C. (2000). Physiological Roles of Trehalose in Bacteria and Yeasts: A Comparative Analysis. *Arch. Microbiol.* 174 (4), 217–224. doi: 10.1007/s002030000192
- Baines, S. D., Chilton, C. H., Crowther, G. S., Todhunter, S. L., Freeman, J., and Wilcox, M. H. (2013). Evaluation of Antimicrobial Activity of Cefaroline Against *Clostridium Difficile* and Propensity to Induce *C. Difficile* Infection in an *In Vitro* Human Gut Model. *J. Antimicrob. Chemother.* 68 (8), 1842–1849. doi: 10.1093/jac/dkt107
- Baines, S. D., Crowther, G. S., Freeman, J., Todhunter, S., Vickers, R., and Wilcox, M. H. (2015). SMT19969 as a Treatment for *Clostridium Difficile* Infection: An Assessment of Antimicrobial Activity Using Conventional Susceptibility Testing and an *In Vitro* Gut Model. *J. Antimicrob. Chemother.* 70 (1), 182–189. doi: 10.1093/jac/dku324
- Baines, S. D., Freeman, J., and Wilcox, M. H. (2005). Effects of Piperacillin/Tazobactam on *Clostridium Difficile* Growth and Toxin Production in a Human Gut Model. *J. Antimicrob. Chemother.* 55 (6), 974–982. doi: 10.1093/jac/dki120
- Baines, S. D., Freeman, J., and Wilcox, M. H. (2009). Tolevamer Is Not Efficacious in the Neutralization of Cytotoxin in a Human Gut Model of *Clostridium Difficile* Infection. *Antimicrob. Agents Chemother.* 53 (5), 2202–2204. doi: 10.1128/AAC.01085-08
- Bateman, A., Martin, M. J., O'Donovan, C., Magrane, M., Alpi, E., Antunes, R., et al. (2017). Uniprot: The Universal Protein Knowledgebase. *Nucleic Acids Res.* 45 (D1), D158–D169. doi: 10.1093/nar/gkw1099
- Battaglioli, E. J., Hale, V. L., Chen, J., Jeraldo, P., Ruiz-Mojica, C., Schmidt, B. A., et al. (2018). *Clostridioides Difficile* Uses Amino Acids Associated With Gut Microbial Dysbiosis in a Subset of Patients With Diarrhea. *Sci. Transl. Med.* 10 (464). doi: 10.1126/scitranslmed.aam7019

AUTHOR CONTRIBUTIONS

AB, TH, and MW conceived and designed the experimental studies. AB, IM, NA, WS, EC, YN, HH, and KB conducted the experiments. IM, SM, DW, and AB analysed the experimental data. AB, IM, NA, and MW wrote the manuscript with additional input from TH, GD, DW, SM, and IM. All authors contributed to the article and approved the submitted version.

FUNDING

This study was supported by funds from Hayashibara Co. Ltd (Effect of trehalose on *C. difficile* infection using the *in vitro* gut model).

ACKNOWLEDGMENTS

We thank Sharie Shearman for technical assistance with the gut model, and Dr Carr and Dr Raynor for preparing the sequencing libraries and performing the sequencing.

SUPPLEMENTARY MATERIAL

The Supplementary Material for this article can be found online at: <https://www.frontiersin.org/articles/10.3389/fcimb.2021.670935/full#supplementary-material>

- Bouillaut, L., Self, W. T., and Sonenshein, A. L. (2013). Proline-Dependent Regulation of *Clostridium Difficile* Stickland Metabolism. *J. Bacteriol.* 195 (4), 844–854. doi: 10.1128/JB.01492-12
- Buchfink, B., Xie, C., and Huson, D. H. (2014). Fast and Sensitive Protein Alignment Using DIAMOND. *Nat. Methods* 12 (1), 59–60. doi: 10.1038/nmeth.3176
- Buckley, A. M., Spencer, J., Candlish, D., Irvine, J. J., and Douce, G. R. (2011). Infection of Hamsters With the UK *Clostridium Difficile* Ribotype 027 Outbreak Strain R20291. *J. Med. Microbiol.* 60 (8), 1174–1180. doi: 10.1099/jmm.0.028514-0
- Chilton, C. H., Crowther, G. S., Baines, S. D., Todhunter, S. L., Freeman, J., Locher, H. H., et al. (2014). *In Vitro* Activity of Cadazolid Against Clinically Relevant *Clostridium Difficile* Isolates and in an *In Vitro* Gut Model of *C. Difficile* Infection. *J. Antimicrob. Chemother.* 69 (3), 697–705. doi: 10.1093/jac/dkt411
- Chilton, C. H., Crowther, G. S., Freeman, J., Todhunter, S. L., Nicholson, S., Longshaw, C. M., et al. (2014). Successful Treatment of Simulated *Clostridium Difficile* Infection in a Human Gut Model by Fidaxomicin First Line and After Vancomycin or Metronidazole Failure. *J. Antimicrob. Chemother.* 69, 451–462. doi: 10.1093/jac/dkt347
- Chilton, C. H., Crowther, G. S., Todhunter, S. L., Ashwin, H., Longshaw, C. M., Karas, A., et al. (2015). Efficacy of Alternative Fidaxomicin Dosing Regimens for Treatment of Simulated *Clostridium Difficile* Infection in an *In Vitro* Human Gut Model. *J. Antimicrob. Chemother.* 70 (9), 2598–2607. doi: 10.1093/jac/dkv156
- Chilton, C. H., Crowther, G. S., Todhunter, S. L., Nicholson, S., Freeman, J., Chesnel, L., et al. (2014). Efficacy of Surotomycin in an *In Vitro* Gut Model of *Clostridium Difficile* Infection. *J. Antimicrob. Chemother.* 69 (9), 2426–2433. doi: 10.1093/jac/dku141
- Chilton, C. H., Freeman, J., Crowther, G. S., Todhunter, S. L., Nicholson, S., and Wilcox, M. H. (2012). Co-Amoxiclav Induces Proliferation and Cytotoxin Production of *Clostridium Difficile* Ribotype 027 in a Human Gut Model. *J. Antimicrob. Chemother.* 67 (4), 951–954. doi: 10.1093/jac/dkr584

- Chung, W., Walker, A. W., Louis, P., Parkhill, J., Vermeiren, J., Bosscher, D., et al. (2016). Modulation of the Human Gut Microbiota by Dietary Fibres Occurs at the Species Level. *BMC Biol.* 14, 3. doi: 10.1186/s12915-015-0224-3
- Collins, J., Danhof, H., and Britton, R. A. (2018a). The Role of Trehalose in the Global Spread of Epidemic *Clostridium Difficile*. *Gut Microbes* 10 (2), 1–6. doi: 10.1080/19490976.2018.1491266
- Collins, J., Robinson, C., Danhof, H., Knetsch, C. W., Van Leeuwen, H. C., Lawley, T. D., et al. (2018b). Dietary Trehalose Enhances Virulence of Epidemic *Clostridium Difficile*. *Nature* 553 (7688), 291–294. doi: 10.1038/nature25178
- Crook, D. W., Sarah Walker, A., Kean, Y., Weiss, K., Cornely, O. A., Miller, M. A., et al. (2012). Fidaxomicin Versus Vancomycin for *Clostridium Difficile* Infection: Meta-analysis of Pivotal Randomized Controlled Trials. *Clin. Infect. Dis.* 55 (SUPPL.2), 93–103. doi: 10.1093/cid/cis499
- Crowther, G. S., Baines, S. D., Todhunter, S. L., Freeman, J., Chilton, C. H., and Wilcox, M. H. (2013). Evaluation of NVB302 Versus Vancomycin Activity in an *In Vitro* Human Gut Model of *Clostridium Difficile* Infection. *J. Antimicrob. Chemother.* 68 (1), 168–176. doi: 10.1093/jac/dks359
- Daquigan, N., Seekatz, A. M., Greathouse, K. L., Young, V. B., and White, J. R. (2017). High-Resolution Profiling of the Gut Microbiome Reveals the Extent of *Clostridium Difficile* Burden. *NPJ Biofilms Microbiomes* 35, 1–8. doi: 10.1038/s41522-017-0043-0
- Darkoh, C., DuPont, H. L., Norris, S. J., and Kaplan, H. B. (2015). Toxin Synthesis by *Clostridium Difficile* Is Regulated Through Quorum Signaling. *MBio* 6 (2), e02569–e02514. doi: 10.1128/mBio.02569-14
- Elbein, A. D., Pan, Y. T., Pastuszak, I., and Carroll, D. (2003). New Insights on Trehalose: A Multifunctional Molecule. *Glycobiology* 13 (4), 17–27. doi: 10.1093/glycob/cwg047
- Eyre, D. W., Didelot, X., Buckley, A. M., Freeman, J., Moura, I. B., Crook, D. W., et al. (2019). *Clostridium Difficile* Trehalose Metabolism Variants Are Common and Not Associated With Adverse Patient Outcomes When Variably Present in the Same Lineage. *EBioMedicine*. 43, 347–355. doi: 10.1016/j.ebiom.2019.04.038
- Fachi, J. L., Felipe, J. D. S., Farias A dos, S., Varga-weisz, P., and Vinolo, M. A. R. (2019). Butyrate Protects Mice From *Clostridium Difficile* -Induced Colitis Through an HIF-1-Dependent Mechanism. *Cell Rep.* 27, 750–761. doi: 10.1016/j.celrep.2019.03.054
- Ferreira, J. A., Wu, K. J., Hryckowian, A. J., Bouley, D. M., Weimer, B. C., and Sonnenburg, J. L. (2014). Gut Microbiota-Produced Succinate Promotes *C. Difficile* Infection After Antibiotic Treatment or Motility Disturbance. *Cell Host Microbe* 16 (6), 770–777. doi: 10.1016/j.chom.2014.11.003
- Food Standards Australia New Zealand (FSANZ) (2003). *Final Assessment Report Application A453: Trehalose as a Novel Food* Vol. May) (FOOD Stand Aust NEW Zeal).
- Freeman, J., Neill, F. J. O., and Wilcox, M. H. (2003). Effects of Cefotaxime and Desacetylcefotaxime Upon *Clostridium Difficile* Proliferation and Toxin Production in a Triple-Stage Chemostat Model of the Human Gut. *J. Antimicrob. Chemother.* 52, 96–102. doi: 10.1093/jac/dkg267
- Girinathan, B., Dibenedetto, N., Worley, J., Peltier, J., Lavin, R., Delaney, D., et al. (2020). The Mechanisms of *In Vivo* Commensal Control of *Clostridioides Difficile* Virulence. *BioRxiv*. doi: 10.1101/2020.01.04.894915
- Hofmann, J. D., Otto, A., Berges, M., Biedendieck, R., Michel, A., Becher, D., et al. (2018). Metabolic Reprogramming of *Clostridioides Difficile* During the Stationary Phase With the Induction of Toxin Production. *Front. Microbiol.* 9, 1970. doi: 10.3389/fmicb.2018.01970
- Hryckowian, A. J., Treuren, W. V., Smits, S. A., Davis, N. M., Gardner, J. O., Bouley, D. M., et al. (2018). Microbiota-Accessible Carbohydrates Suppress *Clostridium Difficile* Infection in a Murine Model. *Nat. Microbiol.* 3, 662–669. doi: 10.1038/s41564-018-0150-6
- Hsiao, A., Ahmed, A. M. S., Subramanian, S., Griffin, N. W., Drewry, L. L., Petri, W. A. Jr., et al. (2014). Members of the Human Gut Microbiota Involved in Recovery From *Vibrio Cholerae* Infection. *Nature* 515, 423. doi: 10.1038/nature13738
- Hufeldt, M. R., Nielsen, D. S., Vogensen, F. K., Midtvedt, T., and Hansen, A. K. (2010). Variation in the Gut Microbiota of Laboratory Mice Is Related to Both Genetic and Environmental Factors. *Comp. Med.* 60 (5), 336–342.
- Huson, D. H., Beier, S., Flade, I., Górska, A., El-Hadidi, M., Mitra, S., et al. (2016). Megan Community Edition - Interactive Exploration and Analysis of Large-Scale Microbiome Sequencing Data. *PLoS Comput. Biol.* 12 (6), 1–12. doi: 10.1371/journal.pcbi.1004957
- Jain, N. K., and Roy, I. (2009). Effect of Trehalose on Protein Structure. *Protein Sci.* 18, 24–36. doi: 10.1002/pro.3
- Jenior, M. L., Leslie, J. L., Young, V. B., and Schloss, P. D. (2017). *Clostridium Difficile* Colonizes Alternative Nutrient Niches During Infection Across Distinct Murine Gut Microbiomes. *mSystems* 2 (4). doi: 10.1128/mSystems.00063-17
- Johnson, S., Louie, T. J., Gerding, D. N., Cornely, O. A., Chasan-Taber, S., Fitts, D., et al. (2014). Vancomycin, Metronidazole, or Tolevamer for *Clostridium Difficile* Infection: Results From Two Multinational, Randomized, Controlled Trials. *Clin. Infect. Dis.* 59 (3), 345–354. doi: 10.1093/cid/ciu313
- Kal, A. J., Zonneveld, A. J. V., Benes, V., Van Den, B. M., Koerkamp, M. G., Albermann, K., et al. (1999). Dynamics of Gene Expression Revealed by Comparison of Serial Analysis of Gene Expression Different Carbon Sources. *Mol. Biol. Cell* 10, 1859–1872. doi: 10.1091/mbc.10.6.1859
- Khanna, S., Montassier, E., Schmidt, B., Patel, R., Knights, D., Pardi, D. S., et al. (2016). Gut Microbiome Predictors of Treatment Response and Recurrence in Primary *Clostridium Difficile* Infection. *Aliment. Pharmacol. Ther.* 44, 715–727. doi: 10.1111/apt.13750
- Kurtz, C. B., Cannon, E. P., Brezzani, A., Pitruzzello, M., Dinardo, C., Rinard, E., et al. (2001). GT160-246, A Toxin Binding Polymer for Treatment of *Clostridium Difficile* Colitis. *Antimicrob. Agents Chemother.* 45 (8), 2340–2347. doi: 10.1128/AAC.45.8.2340-2347.2001
- Lee, A. S. Y., and Song, K. P. (2005). LuxS/Autoinducer-2 Quorum Sensing Molecule Regulates Transcriptional Virulence Gene Expression in *Clostridium Difficile*. *Biochem. Biophys. Res. Commun.* 335 (3), 659–666. doi: 10.1016/j.bbrc.2005.07.131
- Ley, R. E., Backhed, F., Turnbaugh, P., Lozupone, C. A., Knight, R. D., and Gordon, J. I. (2005). Obesity Alters Gut Microbial Ecology. *Proc. Natl. Acad. Sci.* 102 (31), 11070–11075. doi: 10.1073/pnas.0504978102
- Liu, C., Finegold, S. M., Song, Y., and Lawson, P. A. (2008). Reclassification of *Clostridium Coccoides*, *Ruminococcus Hansenii*, *Ruminococcus Hydrogenotrophicus*, *Ruminococcus Luti*, *Ruminococcus Productus* and *Ruminococcus Schinkii* as *Blautia Coccoides* Gen. nov., comb. nov., *Blautia Hansenii*. *Int. J. Syst. Evol. Microbiol.* 58, 1896–1902. doi: 10.1099/ijs.0.65208-0
- Marsh, J. W., Arora, R., Schlackman, J. L., Shutt, K. A., Curry, S. R., and Harrison, L. H. (2012). Association of Relapse of *Clostridium Difficile* Disease With BI/NAP1/027. *J. Clin. Microbiol.* 50 (12), 4078–4082. doi: 10.1128/JCM.02291-12
- Martin, M. (2011). Cutadapt Removes Adapter Sequences From High-Throughput Sequencing Reads. *EMBnet. J* 17 (1), 10. doi: 10.14806/embnet.17.1.200
- Maruta, K., Nakada, T., Kubota, M., Chaen, H., Kurimoto, M., Tsujisaka, Y., et al. (1995). Formation of Trehalose From Maltooligosaccharides by a Novel Enzymatic System. *Biosci. Biotechnol. Biochem.* 8451 (10), 1829–1834. doi: 10.1271/bbb.59.1829
- McDonald, J. A. K., Mullish, B. H., Pechlivanis, A., Liu, Z., Brignardello, J., Kao, D., et al. (2018). Inhibiting Growth of *Clostridioides Difficile* by Restoring Valerate, Produced by the Intestinal Microbiota. *Gastroenterology* 155 (5), 1495–1507.e15. doi: 10.1053/j.gastro.2018.07.014
- Milani, C., Ticinesi, A., Gerritsen, J., Nounvenne, A., Andrea Lugli, G., Mancabelli, L., et al. (2016). Gut Microbiota Composition and *Clostridium Difficile* Infection in Hospitalized Elderly Individuals: A Metagenomic Study. *Sci. Rep.* 6 (March), 1–12. doi: 10.1038/srep25945
- Moura, I. B., Buckley, A. M., Ewin, D., Shearman, S., Clark, E., Wilcox, M. H., et al. (2019). Omadacycline Gut Microbiome Exposure Does Not Induce *Clostridium Difficile* Proliferation or Toxin Production in a Model That Simulates the Proximal, Medial, and Distal Human Colon. *Antimicrob. Agents Chemother.* 63 (2), 1–11. doi: 10.1128/AAC.01581-18
- Murata, T., Yamato, I., and Kakinuma, Y. (2005). Structure and Mechanism of Vacuolar Na⁺ Translocating ATPase From *Enterococcus Hirae*. *J. Bioenerg. Biomembr.* 37 (6), 411–413. doi: 10.1007/s10863-005-9481-0
- Nawrocki, K. L., Wetzel, D., Jones, J. B., Woods, E. C., and McBride, S. M. (2018). Ethanolamine Is a Valuable Nutrient Source That Impacts *Clostridium Difficile* Pathogenesis. *Environ. Microbiol.* 20 (4), 1419–1435. doi: 10.1111/1462-2920.14048
- Nguyen, T. L. A., Vieira-Silva, S., Liston, A., and Raes, J. (2015). How Informative Is the Mouse for Human Gut Microbiota Research? *Dis. Model Mech.* 8, 1–16. doi: 10.1242/dmm.017400
- Petrof, E. O., Gloor, G. B., Vanner, S. J., Weese, S. J., Carter, D., Daigneault, M. C., et al. (2013). Stool Substitute Transplant Therapy for the Eradication of *Clostridium Difficile* Infection: 'Repopulating' the Gut. *Microbiome* 1, 1–12. doi: 10.1186/2049-2618-1-3

- Pinto-bonilla, J. C., Olmo-jimeno, A., Llovet-osuna, F., and Hernández-, E. (2015). A Randomized Crossover Study Comparing Trehalose/Hyaluronate Eyedrops and Standard Treatment: Patient Satisfaction in the Treatment of Dry Eye Syndrome. *Ther. Clin. Risk Manag.* 11, 595–603. doi: 10.2147/TCRM.S77091
- Public Health England (2016). Management of Infection Guidance for Primary Care for Consultation and Local Adaptation About Public Health England 1–75.
- Reeves, A. E., Theriot, C. M., Bergin, I. L., Huffnagle, G. B., Schloss, P. D., and Young, V. B. (2011). The Interplay Between Microbiome Dynamics and Pathogen Dynamics in a Murine Model of *Clostridium Difficile* Infection. *Gut Microbes* 2 (3), 145–158. doi: 10.4161/gmic.2.3.16333
- Robinson, J. I., Weir, W. H., Crowley, J. R., Hink, T., Reske, K. A., Kwon, J. H., et al. (2019). Metabolomic Networks Connect Host-Microbiome Processes to Human Clostridioides Difficile Infections. *J. Clin. Invest.* 129 (9), 3792–3806. doi: 10.1172/JCI126905
- Rognes, T., Flouri, T., Nichols, B., Quince, C., and Mahé, F. (2016). VSEARCH: A Versatile Open Source Tool for Metagenomics. *PeerJ* 4, e2584. doi: 10.7717/peerj.2584
- Rogosa, M. (1964). The Genus Veillonella. *J. Bacteriol.* 87 (1), 162–170. doi: 10.1128/jb.87.1.162-170.1964
- Roychowdhury, S., Cadnum, J., Glueck, B., Obrenovich, M., Donskey, C., Cresci, G. A. M., et al. (2018). *Faecalibacterium Prausnitzii* and a Prebiotic Protect Intestinal Health in a Mouse Model of Antibiotic and *Clostridium Difficile* Exposure. *JPEN J. Parenter. Enteral Nutr.* 42 (7), 1156–1167. doi: 10.1002/jpen.1053
- Rupnik, M., Wilcox, M. H., and Gerding, D. N. (2009). *Clostridium Difficile* Infection: New Developments in Epidemiology and Pathogenesis. *Nat. Rev. Microbiol.* 7 (7), 526–536. doi: 10.1038/nrmicro2164
- Saund, K., Rao, K., Young, V. B., and Snitkin, E. S. (2020). Genetic Determinants of Trehalose Utilization Are Not Associated With Severe *Clostridium Difficile* Infection Outcome. *Open Forum Infect. Dis.*, 7 (1), 1–4. doi: 10.1093/ofid/ofz548
- Saxton, K., Baines, S. D., Freeman, J., O'Connor, R., and Wilcox, M. H. (2009). Effects of Exposure of *Clostridium Difficile* PCR Ribotypes 027 and 001 to Fluoroquinolones in a Human Gut Model. *Antimicrob. Agents Chemother.* 53 (2), 412–420. doi: 10.1128/AAC.00306-08
- Schloss, P. D., Westcott, S. L., Ryabin, T., Hall, J. R., Hartmann, M., Hollister, E. B., et al. (2009). Introducing Mothur: Open-source, Platform-Independent, Community-Supported Software for Describing and Comparing Microbial Communities. *Appl. Environ. Microbiol.* 75 (23), 7537–7541. doi: 10.1128/AEM.01541-09
- Selber-hnativ, S., Rukundo, B., Ahmadi, M., Akoubi, H., Baird, A., Begum, F., et al. (2017). Human Gut Microbiota: Toward an Ecology of Disease 8, July. *Front Microbiol.* 8, 1265 .doi: 10.3389/fmicb.2017.01265
- Sorg, J. A., and Sonenshein, A. L. (2008). Bile Salts and Glycine as Cogerminants for *Clostridium Difficile* Spores. *J. Bacteriol.* 190 (7), 2505–2512. doi: 10.1128/JB.01765-07
- Swanson, R. N., Hardy, D. J., Shipkowitz, N. L., Hanson, C. W., Ramer, N. C., Fernandes, P. B., et al. (1991). *In Vitro* and *In Vivo* Evaluation of Tiacumicins B and C Against *Clostridium Difficile*. *Antimicrob. Agents Chemother.* 35 (6), 1108–1111. doi: 10.1128/AAC.35.6.1108
- Whatmore, A., Chudek, J., and Reed, R. (1990). The Effects of Osmotic Upshock on the Intracellular Solute Pools of *Bacillus Subtilis*. *J. Gen. Microbiol.* 136, 2527–2535. doi: 10.1099/00221287-136-12-2527
- Zhang, Y., and DeBosch, B. J. (2020). Microbial and Metabolic Impacts of Trehalose and Trehalose Analogues. *Gut Microbes* 11 (5), 1475–1482. doi: 10.1080/19490976.2020.1750273

Conflict of Interest: MW has received honoraria for consultancy work, financial support to attend meetings and research funding from Astellas, AstraZeneca, Abbott, Actelion, Alere, AstraZeneca, Bayer, bioMérieux, Cerexa, Cubist, Da Volterra, Durata, Merck, Nabriva Therapeutics plc, Pfizer, Qiagen, Roche, Seres Therapeutics Inc., Synthetic Biologics, Summit and The Medicines Company. IBM has received support to attend meetings from Techlabs Inc. AB has received research funding from Seres Therapeutics Inc., Motif Biosciences plc., Nabriva Therapeutics plc, Tetrphase Pharmaceuticals, and Hayashibara Co. Ltd. Authors NA, YN and TH were employed by Hayashibara Co. Ltd./NAGASE Group.

The authors declare that this study received funding from Hayashibara Co. Ltd. The funder had the following involvement in the study: measuring trehalose and glucose concentrations from each vessel in all of the gut models by HPLC.

The remaining authors declare that the research was conducted in the absence of any commercial or financial relationships that could be construed as a potential conflict of interest.

Copyright © 2021 Buckley, Moura, Arai, Spittal, Clark, Nishida, Harris, Bentley, Davis, Wang, Mitra, Higashiyama and Wilcox. This is an open-access article distributed under the terms of the Creative Commons Attribution License (CC BY). The use, distribution or reproduction in other forums is permitted, provided the original author(s) and the copyright owner(s) are credited and that the original publication in this journal is cited, in accordance with accepted academic practice. No use, distribution or reproduction is permitted which does not comply with these terms.